Measuring Short-term Voltage Stability of Power Systems Dominated by Inverter-based Resources Part II: Port-wise Generalized Voltage Damping Index

Xiaoyu Peng, Feng Liu, Peng Yang, Beisi Tan, Pengfei Gao, and Zhaojian Wang

***Abstract*—In Part I of this paper, we have proposed the new concept of generalized voltage damping (GVD) and derived the system-wise GVD (sGVD) index for the global assessment of voltage stability and system strength. Part II of this paper extends this concept to develop a port-wise index for quantifying the voltage damping characteristics locally. To this end, we decompose the sGVD index into individual ports (or buses), thereby forming the port-wise GVD (pGVD) index, which can be computed using local measurements. By inheriting the interpretation of the system-wise index, we further prove that the average of pGVD indices across all ports is approximately identical to the sGVD index. Moreover, it exhibits favorable properties absent in existing indices based on the maximum Lyapunov exponents (MLEs) of terminal voltages, empowering its application as an assessment metric for the supportive capability of devices to short-term voltage stability. The model-independent feature enables the assessment considering the complex and nonlinear dynamics of inverter-based resources (IBRs) such as wind turbines, photovoltaics (PVs), and battery energy storages. Experimental simulations conducted on a heterogeneous IEEE 39-bus system and two practical power systems with massive renewable resource integration confirm the theoretical results. The influence of voltage control strategies of IBR, control parameters, integration locations, and active power control parameters are also analyzed, providing a new perspective for understanding the individual support of devices for short-term voltage stability.**

***Index Terms*—Voltage stability, voltage damping, maximum Lyapunov exponent (MLE), inverter-based resource (IBR), inverter-dominant power system.**

I. Introduction

PART I of this two-part paper has introduced the concept of generalized voltage damping (GVD) and derived the system-wise GVD (sGVD) index, characterizing the voltage stability and system strength from a global perspective. Regarding the locality nature of voltage issues in power systems [1], in Part II of this paper, we extend the proposed concept of GVD to address the issue of short-term voltage stability (STVS) assessment from a local perspective.

Local analysis of STVS has practical significance. To combat the increasing risk of voltage instability, inverter-based resources (IBRs) such as wind turbines, photovoltaics (PVs), and battery energy storages are generally required to have fault ride-through capability and even provide active voltage support [2]. The voltage dynamics of these IBRs are usually heterogeneous and sometimes are even pure data-driven or gray-box without accessible analytical expressions, hindering a quantitative mechanism-based comparison of STVS support provided by different IBRs. Therefore, a uniform assessment of STVS device supports during transience is crucial in evaluating the effectiveness of designed voltage control and attributing responsibility for instabilities [3], [4]. Additionally, voltage support has the potential to be the auxiliary service provided by devices to the grid and thus the precise assessment is fundamental for fair incentives. This paper refers to this issue as the voltage supportive capability assessment of devices to power systems.

There are generally two methods to assessing STVS supportive capability: mechanism-based and measurement-based methods. Mechanism-based methods take advantage of clear physical interpretation. For example, [5] derives a voltage inertia index from the flux link reaction process, quantifying the support of devices to initial voltage sag. However, it is only applicable to rotating machines due to its model restriction. The stability condition of droop-controlled inverter-interfaced grids is obtained in [6] and the criteria margin can be viewed as the relative support provided by the devices. Similarly, the transient support of IBRs with dispatchable virtual oscillator control can be quantifIed by comparing the node passivity and the network passivity shortage in a distributed manner [7]. However, these methods rely on specif-

Manuscript received: December 5, 2024; revised: March 3, 2025; accepted: May 5, 2025. Date of CrossCheck: May 5, 2025. Date of online publication: July 7, 2025.

This work was supported by the Science and Technology Project of State Grid Corporation of China (No. 5100-202499008A-1-1-ZN).

X. Peng and F. Liu (corresponding author) are with the Department of Electrical Engineering, Tsinghua University, Beijing, China (e-mail: pengxy19@tsinghua.org.cn; lfeng@tsinghua.edu.cn).

P. Yang is with the School of Electronics and Information, Xi'an Polytechnic University, Xi'an, China (e-mail: p-yang13@tsinghua.org.cn).

B. Tan and P. Gao are with the North China Branch, State Grid Corporation of China, Beijing, China (e-mail: 1025782048@qq.com; gpf_cepri@163.com).

Z. Wang is with the Department of Automation, Shanghai Jiao Tong University, Shanghai, China (e-mail: wangzhaojian@sjtu.edu.cn).

DOI: 10.35833/MPCE.2024.001298

ic IBR models and assumptions for the convenience of theoretical analysis. Conversely, the transient energy description enables a more adaptable analysis. In [8], a generalized Dirac structure of power systems is revealed, which motivates that the supportive capability of devices could be depicted by its transient energy exchange on a port. Furthermore, [9] and [10] have developed quantitative indices based on the transient energy dissipation process. These methods consider both device and network parameters, providing some admirable insights into the STVS mechanism. Despite many advantages, these mechanism-based methods are built upon strict models and assumptions. Hence, nonlinear factors like limiters [11] and nonlinear control curves [12], which are practical issues for IBRs, are disregarded. Besides, the system operators might not obtain the exact model of some IBRs due to confidentiality and time-varying characteristics. Both facts hinder the accuracy and reliability of assessments.

An alternative method based on measurements relies much less on specific models and assumptions. One of the most widely used indices is derived by comparing the difference between measured and predetermined terminal voltage curves and then quantified by the integration along time [13], [14]. Such indices are easy to understand and have been widely used to assess the effectiveness of voltage control strategies [15], as well as guide the planning of dynamic reactive power sources [16]. Additionally, further methods have been reported to process voltage curves with theories such as Shapelet classification [17] and maximum Lyapunov exponent (MLE) [18], [19]. However, as analyzed in Part I of this paper, voltage transience is jointly determined by the device dynamics and its interaction with others through the network. Therefore, the methods based on voltage measurements may fail to distinguish these contributors and provide incomprehensive or even misleading assessment results. Essentially, terminal voltages do not directly correspond to the stability mechanisms nor correctly reflect the actual supportive capability of devices. Most recently, hybrid methods have been devised to take advantage of mechanism-based and measurement-based methods together, but they still impose strict restrictions on the models of devices, especially dynamic loads, for the sake of interpretability [20], [21].

To address this problem, this part extends the idea from Part I to characterize the STVS supportive capability of devices from the energy perspective. Similar to the interpretation of the system-wise index, we derive a port-wise GVD (pGVD) index to quantify the dissipation rate of voltage transient energy (VTE) at the device level, which physically reflects its support to STVS. The main contributions are twofold.

1) Theory: the pGVD index is derived by decomposing the system-wise sGVD, proposed in Part I of this paper [1]. We prove that sGVD is approximately the average of pGVD indices across all ports of the power system, providing pGVD with a clear and solid interpretation. Additionally, the computation of pGVD relies only on local measurements on a port, enabling a model-free and distributed assessment of STVS at the device level.

2) Application: the proposed pGVD index is applied to measure the STVS supportive capability provided by (aggregate) devices. The analysis indicates that the index possesses some unique properties including averaging representation, monotonic correlation, and weak coupling, distinguishing it from current voltage-measurement-based MLE indices. Thanks to these appealing properties, pGVD provides a measurement-based method to quantify the individual contribution of IBRs on supporting STVS with consideration of various nonlinear dynamics.

The rest of the paper is organized as follows. In Section II, the definition of the pGVD index is provided with interpretation. Then, the index is applied to STVS supportive capability assessment in Section III. Section IV verifies the results on a modified heterogeneous IEEE 39-bus system and two practical power systems with massive renewable resources integrated with inverter interfaces. Section V discusses the relationship between the proposed index and existing indices and demonstrates an assessment framework combining both advantages. Finally, Section VI concludes the paper.

II. pGVD Index

In this paper, we use the same notations as in Part I. Specifically, we consider a n-bus power system $\mathcal{G}=G(\mathcal{V},\mathcal{E})$. where $\mathcal{V}$ and $\mathcal{E}$ denote the sets of buses and transmission lines, respectively. Each bus $i\in\mathcal{V}$ is represented from the integrating port by (V_i,θ_i,P_i,Q_i), where the four entries denote voltage amplitude, phase angle, active power, and reactive power, respectively. The voltage dynamics of the device $i\in\mathcal{V}$ satisfy the following, which is the same as Part I of this paper.

$$\tau_i\frac{\mathrm{d}V_i}{\mathrm{d}t}=-k_iV_i+u_i-\frac{Q_i}{V_i} \tag{1}$$

where τ_i, u_i, and k_i are the voltage time constant, steady-value regulation, and voltage damping coefficient, respectively.

We also continue the key assumptions from Part I. Lastly, similar to the first part, we remind the readers that the validity of the proposed pGVD index does not rely on these assumptions and specific models since it inherits the model-free nature of the sGVD index. In actual index computation and time-domain simulations, the model and assumption restrictions are not employed.

A. Definition of pGVD Index

As introduced in Part I, the calculation of sGVD relies on a centralized algorithm since it is essentially a system-level index. However, in addition to the voltage damping exhibited by the overall system, we are also interested in the voltage damping provided by each (aggregate) device, which inspires a device-level concept, i.e., the pGVD index. The construction of pGVD index based on sGVD index is demonstrated in Fig. 1 and the rigorous definition is given in Definition 1.

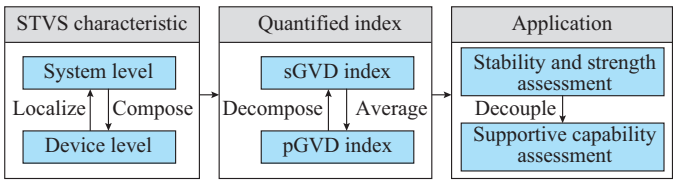

Fig. 1. Construction of pGVD index based on sGVD index.

Definition 1 (pGVD index) The pGVD index $K_V^{(i)}$ of the port $i \in \mathcal{V}$ is defined in (2). The VTE and MLE are defined in Part I.

$$K_V^{(i)} = -MLE(VTE^{(i)}) \tag{2}$$

The pGVD index is locally defined on the port information. Compared with the sGVD index, it reflects the VTE dissipative capability of a given port, which might represent one or multiple devices, or even the external grids.

B. Rationale of Proposed pGVD Index: Simple Cases

Here, we explain the rationale of the pGVD index by showing its analytic expressions considering simple device dynamics.

1) Device in single-machine-infinite-bus (SMIB) system. In this situation, Theorem 1 indicates that the pGVD reflects the supportive capability of voltage control of the device, which is the same as Theorem 1 of Part I.

Theorem 1 Suppose Assumptions 1 and 2 in Part I hold for an SMIB system with the device dynamics (1). If the voltage damping coefficient $k_i > 0$, then, the pGVD index is:

$$K_V^{(i)} = \frac{k_i + 1/X}{\tau_i} \tag{3}$$

where X is the transmission line reactance defined in Part I of this paper.

2) Zero-reactive-power device. In this situation, the port neither injects into nor consumes reactive power from the grid. In practice, it is the case when some devices, like PVs and energy storage systems, are operating with a power factor of one. Besides, a transit bus without any connected devices can be viewed as a virtual port with zero-reactive-power injection.

Theorem 2 The pGVD index of a zero-reactive-power device is zero, i.e., $K_V^{(i)} = 0$ if $Q_i(t) \equiv 0$ for $\forall t > 0$.

It is easy to prove the theorem by noticing $VTE^{(i)} = \int Q_i / V_i \mathrm{d}V_i \equiv 0$, and hence $VTE^{(i)}(t)$ does not decay. It is worth noting that the theorem does not rely on the specific form of device voltage dynamics, which reflects the interesting nature of the pGVD index, as discussed below.

Remark 1 Theorem 2 indicates that devices without reactive power injection do not provide voltage damping to support STVS in the sense of the pGVD index. This result matches our common understanding. In contrast, directly computing the MLE of port voltages, which is widely adopted in the existing literature [17], [18], [22], does not have this property. For instance, we consider a connecting bus as a special case. It does not consume from or inject the power into the grid and thus shall not contribute to support STVS, as indicated by the zero value of the pGVD index. However, since the voltage dynamic on this bus always exists, MLE is generally non-zero. Therefore, we argue that the voltage-based MLE indices do not truly reflect the supportive capability of a port. Indeed, its "support" is mainly provided by other nearby devices through network coupling, which has been discussed in Part I. In this context, the pGVD index may better characterize voltage damping from the perspective of transient energy dissipation. This issue will be further discussed in the next section.

C. Rationale of pGVD Index: Relationship with sGVD

This subsection examines the relationship between system-wise and port-wise indices. Considering that the pGVD and sGVD indices measure the voltage damping of each port and the overall system, respectively, a natural question arises: is there a quantitative relationship between them? Here, we reveal that, under certain conditions, the sGVD index is approximately the average of pGVD indices.

Theorem 3 Considering an n-bus system, suppose its sGVD and pGVD indices are calculated with Algorithm 1 and Algorithm 2, respectively, as described in Part I with the same regulation parameters α and β, time internal Δt, and window size N. Then, the calculated value of sGVD index $K_V(k\Delta t)$ along with pGVD indices $K_V^{(i)}(k\Delta t)$ for $i \in \mathcal{V}$ at time $t = k\Delta t$ (k denotes the k^{th} time internal in the algorithm) satisfies:

$$\frac{1}{k\Delta t} \ln \frac{\alpha}{\beta} \geq K_V(k\Delta t) - \frac{1}{n} \sum_{i \in \mathcal{V}} K_V^{(i)}(k\Delta t) \tag{4}$$

Additionally, if the VTE at all ports $i \in \mathcal{V}$ further satisfies (5), where $m = \{N+1, N+2, \cdots, N+k\}$, then, (6) also holds.

$$\beta < \left| VTE^{(i)}(m\Delta t) - VTE^{(i)}((m-1)\Delta t) \right| < \alpha \tag{5}$$

$$K_V(k\Delta t) - \frac{1}{n} \sum_{i \in \mathcal{V}} K_V^{(i)}(k\Delta t) \geq -\frac{1}{k\Delta t} \left(\ln \frac{\alpha}{\beta} + \frac{1}{2\beta^2} \right) \tag{6}$$

The proof of Theorem 3 can be found in Supplementary Material A. According to Theorem 5 of Part I, the voltage dynamics converge if the sGVD index $K_V > 0$. Hence, one can find appropriate bounded α and β such that the conditions of Theorem 3 are satisfied. Additionally, based on the definition of MLE, the calculated value of MLE approaches its exact value as $t \to \infty$. Combining (4) and (6) indicates that the sGVD index is approximated by the average of the pGVD indices, provided t is sufficiently large. As a result, for a stable system, we have:

$$K_V \approx \frac{1}{n} \sum_{i \in \mathcal{V}} K_V^{(i)} \tag{7}$$

Remark 2 The approximation (7) reveals an interesting insight. That is, the voltage damping of the system (measured by the sGVD index) is established by the voltage dampings of all individual ports (measured by the pGVD index) through averaging. Recalling the relationship between the sGVD index and system strength analyzed in Part I, this finding explains how system strength is built upon the supportive capabilities of all connected devices. In addition, this result allows us to compare the system-wise and port-wise indices directly, solving the compatibility problem introduced in Part I.

III. STVS Supportive Capability Assessment

In this section, we apply the pGVD index for STVS supportive capability assessment. As introduced before, the procedure is model-independent and thus is compatible with heterogeneous IBRs including traditional synchronous generators (SGs), wind turbines, and PV stations.

A. Outline of Supportive Capability Assessment

The procedure of supportive capability assessment based on the pGVD index is presented in Fig. 2. Firstly, each device measures its voltage and reactive power on the integration port by leveraging phasor measurement units (PMUs). Once a large disturbance is detected, the local assessment program is started. The local assessment program follows these steps: ① VTE is calculated using its definition; ② pGVD index is calculated by Algorithm 2 introduced in Part I; and ③ pGVD index is used for assessing the STVS supportive capability. Then, if necessary, the control center performs a system strength assessment after collecting pGVD indices from all ports.

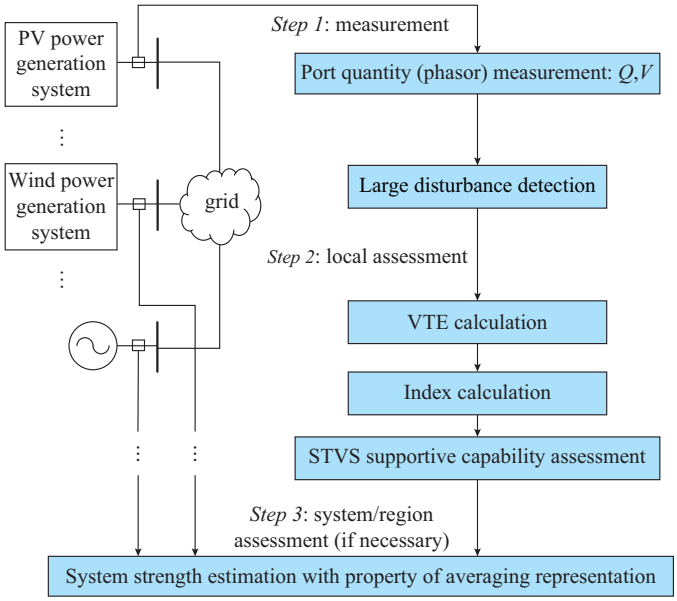

Fig. 2. Procedure of supportive capability assessment based on pGVD index.

B. Property of Averaging Representation

As indicated in Theorem 3, sGVD is approximated by the average of pGVDs, as depicted in (7). This relationship is referred to as the property of averaging representation. In addition to its aforementioned insights, the property indicates that a higher pGVD index implies a greater contribution to the sGVD index of the overall system, indicating stronger support for the system. Thus, this property lays a theoretic foundation for applying the pGVD index to measure the supportive capability of each port.

Figure 3 illustrates the results on a 3-bus system (see details in Supplementary Material B). The curve of sGVD index $K_V(k\Delta t)$ at different time $t=k\Delta t$ is drawn in blue, while the average of pGVD indices for all ports $1/3\sum_{i=1}^{3}K_V^{(i)}(k\Delta t)$ is drawn in red. It is observed that both curves almost converge to the same value as the time $t=k\Delta t$ is sufficiently large, which verifies the property of averaging representation. Additionally, the convergence rate of $1/3\sum_{i=1}^{3}K_V^{(i)}(k\Delta t)$ is almost the same as that of $K_V(k\Delta t)$. Lastly, we note that the approximation is only valid for stable systems, while its extension for unstable systems will be discussed in Supplementary Material C.

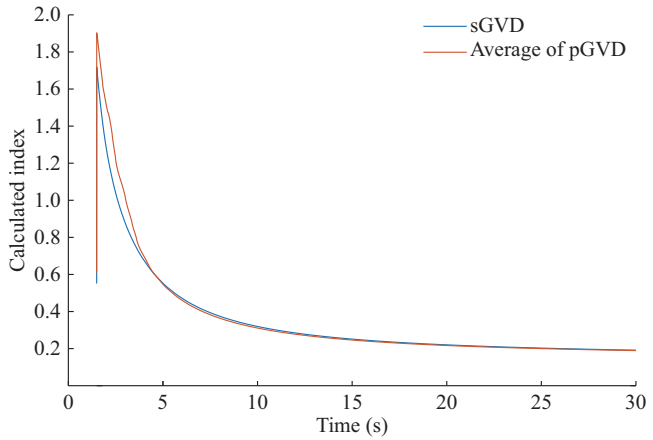

Fig. 3. Property of averaging representation verified on 3-bus system.

Remark 3 Theoretically, Theorem 3 does not impose any requirements on the number of buses n, thus (7) should hold for power systems with an arbitrary n-bus system. However, when n is sufficiently large, the local balancing characteristic of reactive power may deviate. This phenomenon can be roughly explained as follows. Mathematically, if considering the voltage recovery dynamic as a combination of exponential terms (see the proof of Theorem 2 in Part I) written as (8), then its coefficients c_i differ significantly among remote buses due to the spatial characteristics of the voltage dynamics.

$$V_i(t)=\sum_j c_{ij}\exp(\lambda_j t)+d_i \tag{8}$$

where c_{ij}, λ_j, and d_i are the coefficients to describe the voltage dynamics.

This leads to large distinctions in the corresponding parameters α_i and β_i when computing the pGVD index for each port with Algorithm 2, resulting in a larger $\alpha=\max_i\alpha_i$ and smaller $\beta=\min_i\beta_i$ to satisfy the condition of Theorem 3. Therefore, the terms bounded by α and β on the left side of (4) and the right side of (6) will be amplified, causing the slower convergence speed or even divergence. With these considerations, it is recommended to use the property of averaging representation in strongly coupled regions. In a practical hierarchical voltage control architecture, the assessment and control of voltage are performed by different regions, which does not remarkably affect the generality of its application.

C. Property of Monotonic Correlation

The property of monotonic correlation refers to the fact that if all devices satisfy the voltage dynamic (1), then increasing their voltage damping coefficients k_i simultaneously enhances their pGVD indices. For illustration, the voltage damping coefficients in the 3-bus system are set to the same value k. As k increases, the pGVD indices measured from all ports increase monotonically, as shown in Fig. 4.

This property can be understood by noting that both indices reflect the dissipation capability of devices as analyzed previously. Mathematically, it can be derived from the proof of Theorem 2 in Part I. Under the same condition, we have:

$$\min_{j\in\mathcal{V}}\frac{k_j}{\tau_j}\le K_V^{(i)}\le\min_{j\in\mathcal{V}}\frac{k_j-B_{jj}}{\tau_j}\quad\forall i\in\mathcal{V}\tag{9}$$

where B_{jj} is the $(j,j)^{\text{th}}$ element of the susceptance matrix $\boldsymbol{B}$.

Therefore, its bounds, especially the lower bound, monotonically vary with k. Besides, the different increasing ratios in Fig. 4 could also be explained by the formula, since voltage damping is influenced by not only the voltage damping coefficient k but also the time constant τ. Note that in Fig. 4, pGVD1, pGVD2, and pGVD3 represent the pGVD indices measured from buses 1, 2, and 3, respectively.

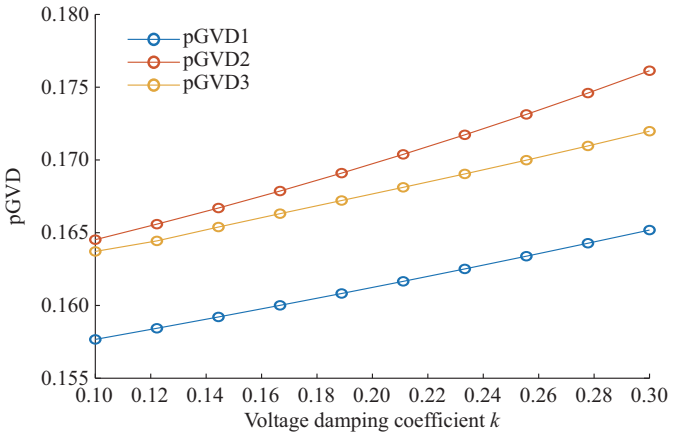

Fig. 4. Property of monotonic correlation verified on 3-bus system.

D. Property of Weak Coupling

The property of weak coupling refers to the fact that pGVD index $K_V^{(i)}$ of a specific port i is mainly influenced by its own dynamic parameters and the influence from other ports is relatively weak.

Figure 5(a) illustrates that the pGVD indices of three ports vary with the parameter k_2 of IBR2. As k_2 increases, only the pGVD index of port 2 increases significantly, while the indices of ports 1 and 3 remain almost unchanged. Furthermore, during the sweeping process of k_2, where $k_2=0.1$ - $0.3<0.5=k_3$, it is theoretically expected that $K_V^{(2)}$ should always be less than $K_V^{(3)}$ since $\tau_2\approx\tau_3$, which has also been confirmed by Fig. 5(a). Figure 5(b) and (c) displays the VTE dissipated by each port when $k_2=0.1$ and $k_2=0.3$, respectively, where VTE1, VTE2, and VTE3 represent the VTE sequences measured from the buses 1, 2, and 3, respectively. Three facts regarding the VTE curves are worth noting. Firstly, port 2 dissipates VTE almost completely within 1 s when $k_2=0.3$, whereas the dissipation is not completed within the first 10 s when $k_2=0.1$. Secondly, it can be observed that the VTE dissipation rate of port 3 remains approximately unchanged. Thirdly, the dissipation rate of port 1 has increased but not as much as that of port 2. In summary, the dissipation characteristics are consistent with the result reflected by its pGVD index. Furthermore, it is noteworthy that the VTE dissipation is not necessarily completely monotonic (e.g., as observed in ports 2 and 3 in Fig.5(c)), which might be attributed to voltage control or non-zero transfer conductance in the network. However, the pGVD index reflects the voltage damping throughout the entire transient process.

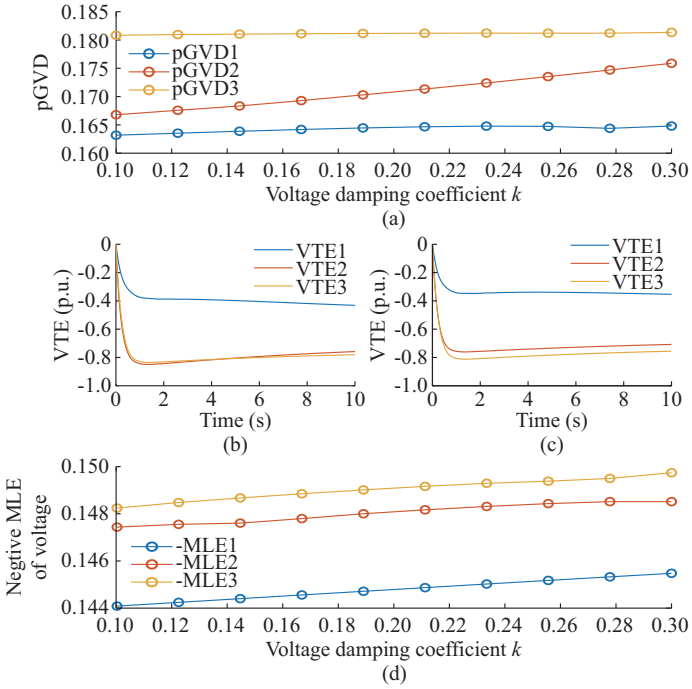

Fig. 5. Property of weak coupling verified on 3-bus system. (a) pGVD indices of different devices. (b) VTE dissipation for $k_2=0.1$. (c) VTE dissipation for $k_2=0.3$. (d) Negative MLE of voltage of different devices.

On the contrary, if the MLE of terminal voltage $-MLE(V_i)$ is used as the index to assess the supportive capability, its relationship with k_2 is quite different, as shown in Fig. 5(d). In Fig. 5(d), MLE1, MLE2, and MLE3 represent the MLEs of terminal voltages measured from the buses 1, 2 and 3, respectively. Some existing literature suggests that $-MLE(V_i)$ can be used to identify vulnerable buses [18], [19], which implicitly recognizes that the MLE of voltage is the reflection of supportive capability. However, according to Fig. 5(d), $-MLE(V_i)$ may not correctly quantify individual voltage supportive capabilities, since changing the control parameters of a specific device, i. e., k_2, will result in almost the same change rate of $-MLE(V_i)$ for all buses. Hence, it is difficult to identify essential devices that truly contribute to the voltage support. That is party why we replace terminal voltages with VTEs in MLE.

We further explain the distinct behaviors of the pGVD index from physical and numerical perspectives as follows.

1) Physical perspective: as previously mentioned, the pGVD index characterizes voltage dynamics from an energy perspective with the combined information of voltage and power injection, thus bringing a more comprehensive reflection of the STVS nature compared with the indices based only on voltage information. For the 3-bus system, the typical power flow between ports 1 and 2 is significantly heavier than that between ports 2 and 3, as shown in Supplementary Material B Fig. SB1. Therefore, according to common understanding, if the voltage supportive capabilities of the other devices change following the control change of port 2, the change rate of port 1 should be greater than that of port 3, since they are more closely connected. The result of the pGVD index in Fig. 5(a) confirms this hypothesis, whereas

the MLE of voltage fails on that because of stronger coupling of voltage dynamics as shown in Fig. 5(d).

2) Numerical perspective: an interesting fact is that with the assumption introduced in Part I, if MLE is computed by the theoretical definition, the pGVD indices of all ports should be the same. Consequently, the property of weak coupling would not manifest. A brief answer is that the property arises from the truncation error due to $k\Delta t \neq \infty$ in Algorithm 2. The different algebraic structures between terminal voltage and VTE further lead to their distinct behaviors.

To illustrate that, we consider the voltage dynamic as the combination of exponential terms as explained previously. For simplicity, we assume that the voltage dynamic of each port is dominated by the same mode $\lambda < 0$. That is, for each $i \in \mathcal{V}$, we can obtain:

$$V_i(t) = c_i \exp(\lambda t) + d_i \tag{10}$$

It is obvious that the MLE of V_i is exactly λ, which is independent of the truncation error of Algorithm 2. In contrast, the MLE of VTE equals λ only if $k\Delta t = \infty$, as shown in (11).

$$\begin{aligned} -MLE(VTE^{(i)}, k\Delta t) = \\ -\frac{1}{k\Delta t}\ln\frac{\gamma_i c_i e^{2\lambda k\Delta t}(e^{2\lambda\Delta t}-1)/2 + \delta_i c_i e^{\lambda k\Delta t}(e^{\lambda\Delta t}-1)}{\gamma_i c_i (e^{2\lambda\Delta t}-1)/2 + \delta_i c_i (e^{\lambda\Delta t}-1)} \approx \lambda + \\ \frac{1}{k\Delta t}\ln\frac{\gamma_i e^{\lambda k\Delta t}+\delta_i}{\gamma_i+\delta_i} \overset{\text{def}}{=} \lambda + \frac{1}{k\Delta t}F(\gamma_i, \delta_i) \end{aligned} \tag{11}$$

where $VTE^{(i)}$ is calculated by substituting (10) into the definition of VTE and the constant parameters $\gamma_i = \sum_i B_{ij}\cos\theta_{ij} c_j$ and $\delta_i = \sum_i B_{ij}\cos\theta_{ij} d_j$; and $F(\gamma_i, \delta_i) = \ln(\gamma_i e^{\lambda k\Delta t} + \delta_i) - \ln(\gamma_i + \delta_i)$. The generation of (11) also employs $e^{\lambda\Delta t} - 1 \approx \lambda\Delta t$ as $\Delta t \approx 0$. This equation explains the relatively large difference between pGVD indices.

Then, we turn to explain why the sensitivity to device voltage dynamics presents to be different for the pGVD index and MLE of terminal voltage. The fact observed in Fig. 5(a) and (d) can be expressed mathematically as:

$$\frac{\partial MLE(VTE^{(i)}, k\Delta t)/\partial k_i}{\partial MLE(VTE^{(i)}, k\Delta t)/\partial k_j} > \frac{\partial MLE(V_i, k\Delta t)/\partial k_i}{\partial MLE(V_i, k\Delta t)/\partial k_j} \tag{12}$$

The inequality means the relative sensitivity of sGVD to the control parameter of its own port is larger than that of the MLE of terminal voltages. Denote the term $(\partial\lambda/\partial k_i)/(\partial\lambda/\partial k_j) = S_{Vij}$, then, the equivalent form of (12) is:

$$S_{Eij} = \frac{\partial F(\gamma_i, \delta_i)/\partial k_i}{\partial F(\gamma_i, \delta_i)/\partial k_j} > S_{Vij} \tag{13}$$

For instance, the condition is satisfied for $i = 2$ and $j = 3$, where the typical values are $S_{E23} \approx 10^3$ and $S_{V23} \approx 10^0$, which aligns with the simulation result in Fig. 5. Furthermore, the reason behind $S_E > S_V$ is that the construction of VTE, which can be viewed as the recombination of voltages as shown in (14), leads to the specific values of γ_i and δ_i, which dominate the value of $F(\gamma_i, \delta_i)$ as $k\Delta t$ is sufficiently large.

$$VTE^{(i)} = \int \frac{Q_i}{V_i} dV_i = \int \sum_{j\in\mathcal{V}} B_{ij}\cos\theta_{ij} V_j dV_i \tag{14}$$

E. Typical Value of pGVD Index

This subsection discusses the typical values of the pGVD index. Qualitatively, since the pGVD index characterizes the dissipation rate of VTE, a larger pGVD index indicates better voltage support. Furthermore, $pGVD \leq 0$ implies that the device destabilizes the voltage, which must be strictly avoided. A quantitative analysis can be conducted from the following two perspectives.

First, the property of averaging representation can be employed for analysis. As pointed out in Part I of this paper, empirical critical values for the sGVD index are as follows: $\text{sGVD} \leq 0.10$ indicates an extremely weak system; $\text{sGVD} \leq 0.25$ indicates a weak system; and $\text{sGVD} \geq 0.35$ indicates a strong system. Moreover, as discussed in the previous section, the system strength, quantified by the sGVD index, is established by the device supportive capability, quantified by the pGVD indices through property of averaging representation. Therefore, to support a strong system, it is desirable to have $\text{pGVD} \geq 0.35$, while $\text{pGVD} \leq 0.10$ indicates extremely weak support provided by the device.

Second, the relationship between the pGVD index and the voltage recovery dynamics can be analyzed. An extremely slow dynamic might be associated with the fault-induced delayed voltage recovery (FIDVR) problem and thus harm the STVS. According to China's standard [23], the amplitude of terminal voltage should be restored to above 0.8 p.u. within 10 s after disturbance. Similar to the analysis of sGVD index, a larger pGVD index generally indicates a faster voltage recovery rate. As a rough estimation, we still assume the voltage dynamic of port $i \in \mathcal{V}$ satisfies (10) and will recover from the initial value V_i^{init} to the steady value V_i^{steady} after sufficient time. Then, the following inequality should be satisfied.

$$V_i(10) = V_i^{steady} - (V_i^{init} - V_i^{steady})e^{10\lambda} \geq 0.8 \tag{15}$$

The inequality should hold for any given initial voltage $0 < V_i^{init} \leq V_i^{steady}$. We further assume $k\Delta t = \infty$ in (11) and then get $K_V^{(i),crit} = \max(-\lambda) = 0.1609$. It is noted that the voltage dynamics usually take much less than 10 s to recover upon 0.80 p.u., and therefore, the above estimation is conservative.

In summary, typical values of the pGVD index are as follows: $\text{pGVD} \geq 0.35$ indicates strong voltage support; $\text{pGVD} \geq 0.25$ indicates acceptable voltage support; $\text{pGVD} \leq 0.15$ indicates weak support; and $\text{pGVD} \leq 0$ suggests the negative influence on STVS.

IV. Case Studies

This section employs the proposed pGVD index to quantify the STVS supportive capability of devices on the modified IEEE 39-bus system and two practical power systems with heterogeneous device dynamics, which is the same as that in Part I [1]. We refer to Part I for detailed description of the system settings. In the system, the grid-forming (GFM) inverters are controlled by conventional droop (CD) or quadratic droop (QD) as explained in Part I. Besides, grid-following (GFL) inverters are also integrated to compare the effect of different control strategies on pGVD indices.

A. Effect of Control Mode on Supportive Capability

In this subsection, we investigate the effect of control mode, i.e., GFM or GFL, on voltage supportive capability. For the system with default configurations, the pGVD index of each port is calculated and presented by the blue bars in Fig. 6(a). The blue bars show the pGVD indices of all devices while CD1 stays in GFM mode. The setting active and reactive power outputs (P_s, Q_s) of GFL1 and GFL2 are the same as those of the GFM CD5 and QD4, respectively. Their distances to the fault bus are similar, too. However, the pGVD indices of GFL1 and GFL2 are significantly lower than those of the latter, indicating that their capability to provide voltage damping is lower, thereby restricting their ability to support STVS. In fact, although it is hard to characterize quantitatively, recent studies and practices have commonly noticed that the GFM IBRs usually provide stronger transient voltage support compared with the GFL counterparts [24], which aligns with our result here.

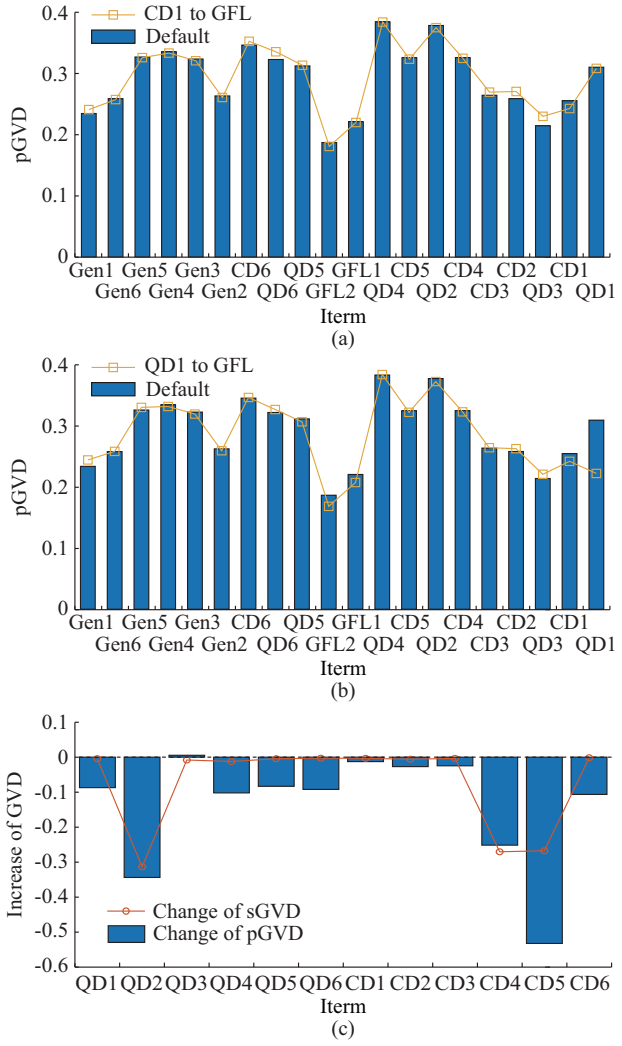

Fig. 6. Effect of control mode on supportive capability. (a) pGVD indices with CD1 in GFM or GFL mode. (b) pGVD indices with QD1 in GFM or GFL mode. (c) Changes of sGVD index and corresponding pGVD index with control mode change on corresponding position.

We now further investigate the effect of control strategies through another experiment. The yellow line in Fig. 6(a) shows the pGVD indices of all devices after transforming the control mode of CD1 from GFM droop to GFL control with its steady power output unchanged. All other device and network settings are consistent with the default one. The pGVD index of the CD1 port drops down after switching to GFL mode, verifying the aforementioned result from another perspective. The yellow line in Fig. 6(b) indicates similar results with transforming the control strategy of QD1, and the decline in the corresponding pGVD index is even greater. Besides, an interesting fact is that the indices of some other nearby GFM devices increase, although slightly, to compensate for the insufficiency.

Lastly, we focus on the change of the pGVD index compared with itself, which is depicted in Fig. 6(c). For example, the orange circle at the CD1 position shows the changes in the sGVD index when the CD1 inverter is changed from GFM to GFL mode. At the same position, the blue bar shows the changes in pGVD index of CD1 with its control switching from GFM to GFL mode. In this sense, it is no surprise that most GFM devices would lose supportive capability if transformed from GFM into GFL mode. Additionally, the sGVD index changes are also drawn with an orange line in Fig. 6(c), all of which are negative. It indicates that the GFL mode could lead to a negative influence on system-wise stability, even if it provides better stability enhancement for some regions.

B. Effect of Control Parameter on Supportive Capability

This subsection investigates the effect of control parameters by changing them solely and observing the varying trend of the pGVD indices. Specifically, the effects of the Q-V droop parameters of CD and QD IBRs are analyzed respectively. Figure 7 presents the test result. In Fig. 7(a), the changes in the pGVD indices of each port are illustrated, when only the droop parameter of CD2 is changed. The pGVD index of CD2 is represented by a blue line, while those of all other devices are represented by gray lines. Similarly, Fig. 7(b)-(f) illustrates changes of the pGVD indices when changing the droop parameter of the IBR CD4 and CD6, as well as QD1, QD3, and QD5, in order. We list several key observations in simulations with helpful insights below.

1) The property of weak coupling still holds in this case. It shows that changing control parameters mainly affects the pGVD index of the local port, indicating that the index well reflects the voltage damping of the device.

2) The pGVD index of a specific port is negatively correlated with the corresponding voltage droop parameters, indicating the strengthened supportive capability for system-wise STVS. This fact has been indicated qualitatively by model-based methods but with strong assumptions on the device model [10]. Furthermore, the fact can be viewed as the extension of the property of monotonic correlation.

3) The sensitivity of the pGVD index to the change of the droop parameter varies for different ports. This phenomenon may be related to other control parameters and the integration location. From a control perspective, this fact means that changing the voltage droop parameters of different IBRs

has different cost-effectiveness ratios for maintaining or enhancing STVS, and thus requires careful consideration.

4) Some abnormal results have also been found. For example, the pGVD index of QD5 does not increase as its droop parameter is less than 0.6, as shown in Fig. 7(c). Physically, $D_{Q\text{-}V} \leq 0.2$ has triggered the power limitation of the IBR, thus the supportive capability of QD5 can be influenced by further decreasing it barely. This fact, inversely, is hard to be captured by theoretical methods especially those built upon small-signal models. The effect of power saturation will be further analyzed in Section IV-D.

Generally, it is difficult for model-based methods to capture strong nonlinearities such as limiting and network coupling in supportive capability assessment. However, since the port VTE naturally contains their influence through voltage and reactive power interactions between devices, the measurement-based method proposed in this paper can take them into consideration. In general, the pGVD index reflects similar findings to some empirical conclusions, which validates the reasonableness of the index itself. Moreover, it takes the advantage of providing a model-free method to directly measure the voltage supportive capability for each port.

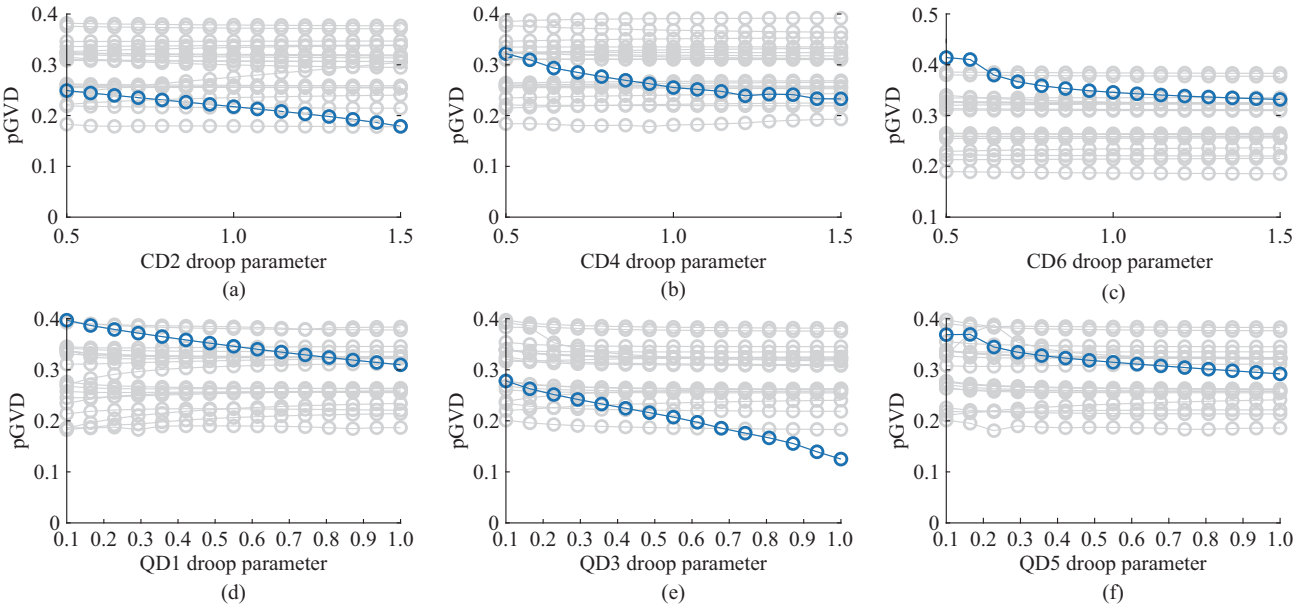

Fig. 7. Effect of *Q-V* droop parameter on supportive capability. (a) CD2 droop parameter with pGVD indices. (b) CD4 droop parameter with pGVD indices. (c) CD6 droop parameter with pGVD indices. (d) QD1 droop parameter with pGVD indices. (e) QD3 droop parameter with pGVD indices. (f) QD5 droop parameter with pGVD indices.

C. Effect of Integration Location on Supportive Capability

In this subsection, we explore the effect of the integration location of devices on their supportive capability. The CD and QD IBRs are still employed as examples. The integration location is characterized by its electrical distance [25] to the fault bus 16. Meanwhile, to eliminate the influence of other factors, we set the identical parameters for the same type of IBRs, which are taken as the average value of the corresponding default values.

The graphical representation in Fig. 8 depicts the relationship between the pGVD indices with their electrical distance to the short-circuit bus. The trend line is generated by the least squares method and represented by a dashed line in the figure. Firstly, the negative slope of trend lines indicates that for the IBRs with the same control strategy and parameters, the closer IBR provides more voltage damping and hence, more support to the STVS of the system. This phenomenon has been suggested by the simple SMIB system case, for which we have the voltage damping coefficient $k_i \propto 1/X$ as calculated in (3). However, we have to note that such a negative correlation relationship only holds on a large scale and may not hold for two specific buses such as CD3 and CD5 in Fig. 8(a). This phenomenon may be related to the nature of power systems as a complex network [26].

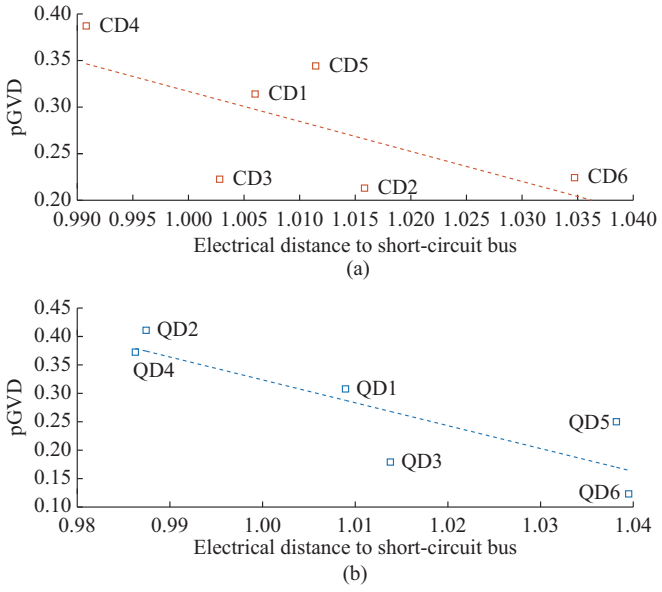

Fig. 8. Effect of integration location on supportive capability. (a) Relationship between CD integrated location with pGVD indices. (b) Relationship between QD integrated location with pGVD indices.

D. Effect of Power Limiter

The saturation characteristics of inverters also influence STVS supportive capability. Due to the highly nonlinear nature of the limiter, performing theoretical analysis is often challenging, particularly in multi-inverter transmission systems. However, since the computation of the proposed pGVD index is based on measurement data, it inherently contains this information. Using the QD5 inverter as an example, its maximum reactive power output is 4.5 p.u.. During the disturbance, the inverter is primarily used for reactive power support, with a peak reactive power output of 4.1 p.u. under default settings. Assuming the reactive power limit is modified, the corresponding reactive power output and pGVD index are shown in Fig. 9. From the figure, it can be observed that the reduction of the reactive power limit (below 4.1 p.u.) decreases the corresponding pGVD index, reflecting a decrease in the voltage supportive capability of the inverter, which aligns with empirical understanding. Furthermore, when the reactive power limit exceeds 4.1 p.u., the limiter no longer operates, resulting in no changes in supportive capability, as also reflected by the corresponding pGVD indices.

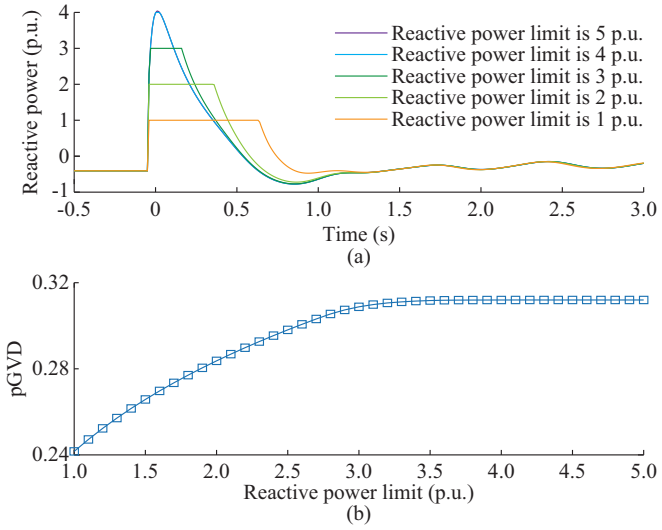

Fig. 9. Effect of power limiter on supportive capability. (a) Reactive power injection under different limits. (b) Relationship between reactive power limit with pGVD index of QD5 IBR.

E. Effect of Active Power Control

When the system approaches voltage collapse, the active power output of devices also significantly affects the STVS. This impact is aptly captured by the proposed pGVD index. As illustrated in Fig. 10, enhancing the active power dynamics through reducing *P-f* droop parameters $D_{P\text{-}f}$ also increases the pGVD index at the corresponding port, even though the voltage control parameters are unchanged. Besides, this impact increases as the system approaches the voltage collapse point (implemented by increasing the clearing time *CT*). This phenomenon occurs because, although active power is not explicitly featured in the VTE and the consequential pGVD index, changes in active power affect the phase angle and voltage dynamics of the system. Hence, the active power can indirectly influence the proposed pGVD index via the expression in (14), i.e., $P \rightarrow (V, \theta) \rightarrow VTE \rightarrow pGVD$ index.

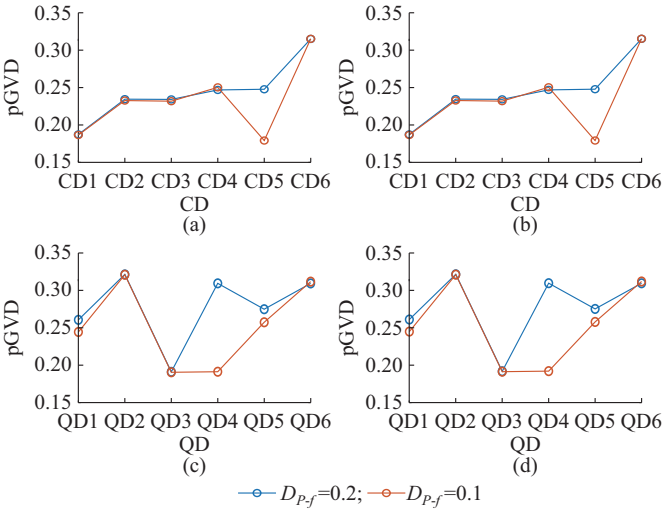

Fig. 10. Effect of active power control parameters on pGVD indices. (a) pGVD indices of CD IBRs as $D_{P\text{-}f}$ changes when CT=0.1 s. (b) pGVD indices of CD IBRs as $D_{P\text{-}f}$ changes when CT=0.15 s. (c) pGVD indices of QD IBRs as $D_{P\text{-}f}$ changes when CT=0.1 s. (d) pGVD indices of QD IBRs as $D_{P\text{-}f}$ changes when CT=0.15 s.

F. Comparison with Classical Methods

This subsection compares the proposed pGVD index with existing supportive capability indices. As outlined in Section I, we examine two categories: mechanism-based and measurement-based, as summarized in Table I. The former includes static indices such as participation factor analysis of the weakest mode of the power flow Jacobi matrix (M1) [27], and dynamic indices such as differential passivity (M2) [10]. The latter includes the voltage-trajectory-measure-based methods (M3, M4) [18], [28] and the proposed pGVD index (M5). The following comparison focuses on two aspects: ① whether the index can accurately and comprehensively capture device dynamic characteristics; and ② whether the index reflects actual supportive capability, namely, whether it reflects the mechanism driving stability restoration.

1) Accuracy and Comprehension

Similar to the procedure described in Sections IV-D, we impose different reactive power saturation on the QD5 IBR. The limiter ensures that it does not exceed its pre-disturbance steady-state level so as not to alter the equilibrium point of the system. The reactive power under different saturation has been provided in Fig. 9(b), clearly demonstrating its impact on the voltage supportive capability of the device. Figure 11 illustrates the comparison of different voltage supportive capability assessment indices (normalized by the value under default settings). Only the measurement-based methods (M3-M5) can accurately capture this effect, whereas the mechanism-based methods (M1 and M2) struggle to do so. In fact, investigating the impact of strong nonlinearities, such as saturation, on large-scale power systems from a theoretical perspective is exceedingly challenging. Such analyses often require making strong assumptions about devices, which can compromise the comprehensiveness and accuracy of supportive capability assessment.

TABLE I
COMPARISON OF DIFFERENT METHODS FOR STVS SUPPORTIVE CAPABILITY ASSESSMENT

Method	Static information	Dynamic information		Model applicability	Reflection of mechanism	Online computation
		Around equilibrium	Far from equilibrium			
M1 (participant factor [27])	√	-	-	√	√	√
M2 (output differential passivity [10])	√	√	∘	∘†	√	√
M3 (voltage trajectory integral [28])	√	√	√	√	-	∘‡
M4 ($MLE(V^{(i)})$ [18])	√	√	√	√	-	∘‡
M5 (proposed pGVD)	√	√	√	√	√	∘‡

Note: √ denotes that the method fully satisfies corresponding characteristics; ∘ denotes that the method partly satisfies corresponding characteristics; - denotes that it is hard for the method to directly handle this characteristic; † denotes that theoretically, the method is suitable for various devices, while the construction of the storage function (or energy function) might be challenging; and ‡ denotes that the two methods mentioned above can achieve online assessment performance while the measurement is used for index computations. If the data are generated by simulations, the assessment speed is restricted by the transient simulation.

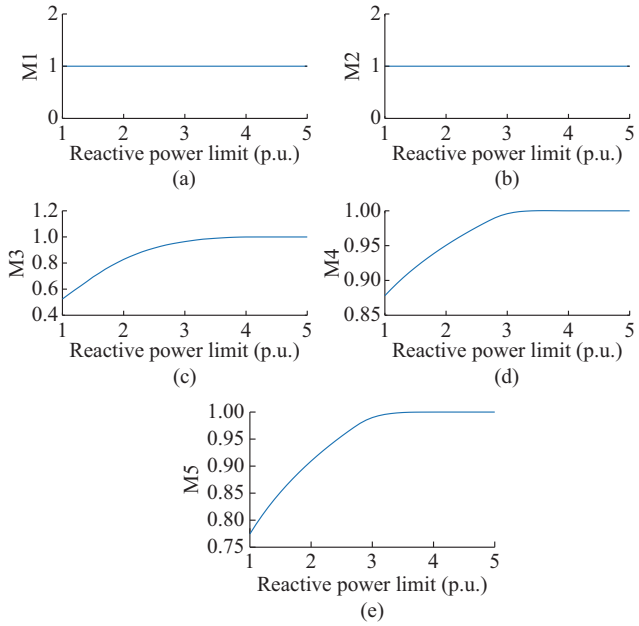

Fig. 11. Comparison of different voltage supportive capability assessment methods. (a) M1. (B) M2. (c) M3. (d) M4. (e) M5.

2) Reflection of Mechanism

For measurement-based indices, we further examine whether they can reflect the actual supportive capability. For illustration, we assume the CD5 IBR is decomposed into two subsystems, each delivering half of the steady-state active power. However, only one subsystem (CD5-A) provides reactive power support, while the other (CD5-B) outputs no reactive power during the whole disturbance. This setup mimics the characteristics of actual renewable energy plants. Despite the renewable energy plant being aggregated as a single node from the perspective of the transmission network, it consists of numerous small-capacity devices with varying reactive supportive capabilities, inter connected through a tight radial grid, as shown in Fig. 12(a). In this situation, we expect that the CD5-B should provide no voltage support or, at best, weaker support than CD5-A. In Fig. 12(b), the supportive capability assessments are presented under the measurement-based methods M3-M5. As analyzed in Section III, despite the significant differences in reactive support control strategies between the two devices, their tight electrical coupling results in nearly identical voltage dynamics as shown in Fig. 12(b). Consequently, M3 and M4, which are based on voltage trajectories, fail to distinguish these differences and provide similar supportive capability assessment for CD5-A and CD5-B (see Table II). In contrast, M5, derived from voltage-related transient energy principles, inherently accounts for the energy differences between devices and, therefore, accurately identifies the disparity between both devices as shown in Table II.

TABLE II
COMPARISON OF M3, M4, AND M5 FOR CD5-A AND CD5-B

Subsystem	M3	M4	M5
CD5-A	0.1253	0.2604	0.3819
CD5-B	0.0971	0.2384	0

G. Further Verification on Practical Power System Models

This subsection investigates the effectiveness of the proposed pGVD index on some practical power systems, including the 71-bus receiving end grid QS-Rece-System and the 2438-bus sending end grid XW-Send-System. The introduction of these systems can be found in Part I of this paper.

1) QS-Rece-System

The pGVD indices of all 525 kV ports in the QS-Rece-System are shown in Supplementary Material D Fig. SD1. We can observe the following results. First, the property of average representation still holds; the average values of the pGVD indices align well with the sGVD index. Second, for devices of the same type, e. g., SG, those located closer to the fault exhibit better support capabilities. Third, synchronous condensers (SCs) show very high pGVD indices, indicating their significant contribution to the STVS of the whole system. Fourth, wind turbines demonstrate better voltage supportive capabilities due to their low voltage ride-through (LVRT) control, whereas PV systems are relatively weaker, which is a fact faithfully reflected by differing pGVD indices.

As mentioned in Part I of this paper, the port-based meth-

od enables hierarchical assessments of STVS supportive capabilities. We illustrate this using the wind power plant WT01, whose grid structure is detailed in Part I. The index $pGVD = 0.427$ can be derived from the voltage magnitude and reactive power injection at its 525 kV terminal B01 as we previously did. Alternatively, the pGVD index can also be calculated by averaging the calculated pGVD indices from all three 38.5 kV collector substations before aggregation, yielding pGVD values of 0.415, 0.443, and 0.392, respectively. Similarly, the pGVD index at each 38.5 kV collector substation can be determined either by averaging the pGVD indices from individual 0.69 kV ports of actual wind turbine or by direct measurement at the 38.5 kV bus. Therefore, the port-based definition makes the proposed pGVD index flexible and scalable.

2) XW-Send-System

The computation of the proposed pGVD index depends solely on measuring the local port on each terminal. Due to its distributed nature, the proposed pGVD index is scalable to large-scale power systems. The assessment relies on minimal computation resources and time as long as the measurement is obtained. For the XW-Send-System, the STVS supportive capability assessment is shown in Supplementary Material D Fig. SD2. For clarity, only active support devices, such as SGs, WTs, and PVs with LVRT capability, are drawn. As long as the simulation data are obtained, the computation of the proposed pGVD index takes less than 0.1 s for each port on a personal computer with intel i5-13400F CPU (2.5 GHz). In practical applications, the simulation is replaced with measurement and thus the index computation is fully applicable for online deployment.

V. Discussions

This section discusses the relationship between the proposed pGVD index and existing indices and demonstrates an assessment framework combining the advantages of both. This paper introduces the concept of the pGVD index, which is derived from decomposing the system-wise voltage damping characteristics into individual ports. Similar to the sGVD index, we note the proposed pGVD index does not tend to supplant current model-based indices but is complementary to each other for a comprehensive assessment of supportive capability of the devices.

The model-based indices are usually easy to compute but not accurate due to model simplification and assumptions for analysis convenience. Therefore, it is more suitable for system planning and online assessment under normal operation conditions, which require fast (but maybe not that precise) evaluation. In this stage, the static analysis such as modal analysis [29], bifurcation analysis [30], and load margin analysis [31] can also be employed. Sufficient static stability is the foundation for a system to maintain STVS following large disturbances. If static analysis indicates the absence of equilibrium points for a given operating condition or that the system is operating in an extremely fragile state, operators should promptly intervene with controls without waiting for precise post-disturbance assessments based on measured data. At the device level, the participation factor analysis of devices in the weakest modal can, to some extent, characterize its contribution to static voltage stability [27].

On the contrary, the pGVD index takes advantage of considering various nonlinear factors of devices but relies on port measurement as we demonstrate in this paper, thus it is more suitable for after-disturbance assessment. In these situations, much more measurement information can be obtained and more precise and comprehensive assessment is required for quantifying supportive capability or attributing instability responsibilities.

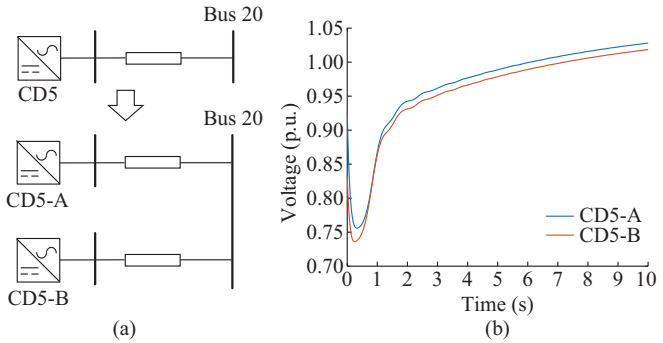

Fig. 12. Splitting of CD5 IBR and terminal voltages of CD5-A and CD5-B. (a) Splitting of CD5 IBR. (b) Terminal voltages of CD5-A and CD5-B.

Therefore, both types of indices can be used at different stages, as shown in Fig. 13. During normal system operation, theory-based methods (including static analysis) are used to quickly, though not precisely, estimate system strength and device supportive capabilities, enabling timely preventive control. After large-signal disturbance happens, a refined assessment is conducted based on the GVD index. Based on these refined assessments, devices with notably insufficient supportive capabilities can be taken offline for retuning or other control adjustments. Additionally, the GVD index results can serve as a metric for indirect incentives: by treating voltage support as an ancillary service, economic incentives can be provided to devices with stronger support capabilities.

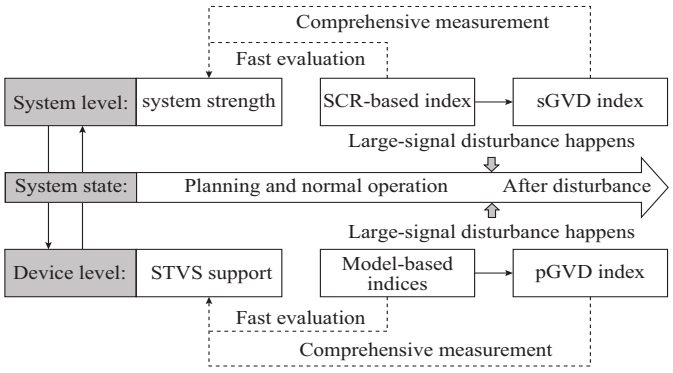

Fig. 13. Relationship between existing indices and GVD indices.

VI. Conclusive Remark

The pGVD index inherits the model-free nature of the sGVD index, requiring only local measurement information for quantifying the voltage-related transient energy dissipa-

tion provided by devices, enabling its compatibility with heterogeneous IBRs with complex and even black-box dynamics. Thanks to its strong physical interpretation and favorable numerical properties, it is demonstrated to be a more reasonable index for assessing individual voltage supportive capability compared with the existing MLE-based indices.

REFERENCES

[1] H. Sun, Q. Guo, J. Qi *et al*., "Review of challenges and research opportunities for voltage control in smart grids," *IEEE Transactions on Power Systems*, vol. 34, no. 4, pp. 2790-2801, Jul. 2019.

[2] M. Islam, M. Nadarajah, and M. J. Hossain, "A grid-support strategy with PV units to boost short-term voltage stability under asymmetrical faults," *IEEE Transactions on Power Systems*, vol. 35, no. 2, pp. 1120-1131, Mar. 2020.

[3] P. G. Estevez, P. Marchi, C. Galarza *et al*., "Complex dissipating energy flow method for forced oscillation source location," *IEEE Transactions on Power Systems*, vol. 37, no. 5, pp. 4141-4144, Sept. 2022.

[4] Z. Lv, B. Wang, Q. Guo *et al*., "Optimal grid-support strategy with inverter-interfaced distributed generators for short-term voltage stability improvement," *IEEE Transactions on Sustainable Energy*, vol. 15, no. 1, pp. 499-512, Jan. 2024.

[5] Y. Lin, H. Ge, B. Wang *et al*. (2022, Jan.). Flux linkage based evaluation method for voltage inertia and voltage recovery capability under large disturbances. [Online]. Available: https://arxiv. org/abs/ 2209.01615

[6] J. Schiffer, R. Ortega, A. Astolfi *et al*., "Conditions for stability of droop-controlled inverter-based microgrids," *Automatica*, vol. 50, no. 10, pp. 2457-2469, Oct. 2014.

[7] X. He and F. Dörfler, "Passivity and decentralized stability conditions for grid-forming converters," *IEEE Transactions on Power Systems*, vol. 39, no. 3, pp. 5447-5450, May 2024.

[8] Y. Li, "Methodology for locating the oscillation sources in power systems based on energy structure," Ph.D. dissertation, Tsinghua Univeristy, Beijing, China, 2013.

[9] P. Vorobev, P.-H. Huang, M. A. Hosani *et al*., "A framework for development of universal rules for microgrids stability and control," in *Proceedings of 2017 IEEE 56th Annual Conference on Decision and Control (CDC)*, Melbourne, Australia, Jun. 2017, pp. 5125-5130.

[10] P. Yang, F. Liu, Z. Wang *et al*., "Distributed stability conditions for power systems with heterogeneous nonlinear bus dynamics," *IEEE Transactions on Power Systems*, vol. 35, no. 3, pp. 2313-2324, May 2020.

[11] X. Wang, H. Wu, X. Wang *et al*., "Transient stability analysis of grid-following vscs considering voltage-dependent current injection during fault ride-through," *IEEE Transactions on Energy Conversion*, vol. 37, no. 4, pp. 2749-2760, Dec. 2022.

[12] Z. Lv, B. Wang, Q. Guo *et al*., "Coordinated optimization for multi-infeed lcc-hvdcs transient control considering short-term voltage stability of receiving-end grid," *IEEE Transactions on Power Systems*, vol. 38, no. 6, pp. 5512-5525, Nov. 2023.

[13] S. Dasgupta, M. Paramasivam, U. Vaidya *et al*., "Entropy-based metric for characterization of delayed voltage recovery," *IEEE Transactions on Power Systems*, vol. 30, no. 5, pp. 2460-2468, Sept. 2015.

[14] W. Zhao, Q. Guo, H. Sun *et al*., "Practical short-term voltage stability index based on voltage curves: definition, verification and case studies," *IET Generation, Transmission & Distribution*, vol. 12, no. 19, pp. 4292-4300, Oct. 2018.

[15] Y. Lin, H. Liu, H. Ge *et al*., "Dimension reduction based short-term voltage security preventive control," in *Proceedings of 2020 IEEE 4th Conference on Energy Internet and Energy System Integration (EI2)*, Wuhan, China, Aug. 2020, pp. 828-833.

[16] J. Qi, W. Huang, K. Sun *et al*., "Optimal placement of dynamic var sources by using empirical controllability covariance," *IEEE Transactions on Power Systems*, vol. 32, no. 1, pp. 240-249, Jan. 2017.

[17] L. Zhu, C. Lu, and Y. Sun, "Time series shapelet classification based online short-term voltage stability assessment," *IEEE Transactions on Power Systems*, vol. 31, no. 2, pp. 1430-1439, Mar. 2016.

[18] S. Dasgupta, M. Paramasivam, U. Vaidya *et al*., "Real-time monitoring of short-term voltage stability using PMU data," *IEEE Transactions on Power Systems*, vol. 28, no. 4, pp. 3702-3711, Nov. 2013.

[19] S. K. Khaitan, "THRUST: a lyapunov exponents based robust stability analysis method for power systems," in *Proceedings of 2017 North American Power Symposium (NAPS)*, Morgantown, USA, Feb. 2017, pp. 1-6.

[20] H. Ge, Q. Guo, H. Sun *et al*., "A model and data hybrid-driven short-term voltage stability real-time monitoring method," *International Journal of Electrical Power & Energy Systems*, vol. 114, p. 105373, Jan. 2020.

[21] X. Zhang, D. J. Hill, and Y. Song, "A load dynamic stability index for short-term voltage stability assessment and control," *IEEE Transactions on Power Systems*, vol. 38, no. 4, pp. 3304-3316, Jul. 2023.

[22] H. Ge, Q. Guo, H. Sun *et al*., "An improved real-time short-term voltage stability monitoring method based on phase rectification," *IEEE Transactions on Power Systems*, vol. 33, no. 1, pp. 1068-1070, Jan. 2018.

[23] *Guides of Power System Voltage Stability Evaluation*, GB/T 40615-2021, 2021.

[24] R. H. Lasseter, Z. Chen, and D. Pattabiraman, "Grid-forming inverters: A critical asset for the power grid," *IEEE Journal of Emerging and Selected Topics in Power Electronics*, vol. 8, no. 2, pp. 925-935, Jun. 2020.

[25] H. Sun, Q. Guo, B. Zhang *et al*., "An adaptive zone-division-based automatic voltage control system with applications in China," *IEEE Transactions on Power Systems*, vol. 28, no. 3, pp. 1816-1828, May 2013.

[26] W. Huang and D. J. Hill, "Network-based analysis of long-term voltage stability considering loads with recovery dynamics," *International Journal of Electrical Power & Energy Systems*, vol. 119, p. 105891, Jul. 2020.

[27] P. S. Kundur, *Power System Stability and Control*. New York: McGraw Hill, 1994.

[28] S. Wildenhues, J. L. Rueda, and I. Erlich, "Optimal allocation and sizing of dynamic var sources using heuristic optimization," *IEEE Transactions on Power Systems*, vol. 30, no. 5, pp. 2538-2546, Sept. 2015.

[29] B. Gao, G. Morison, and P. Kundur, "Voltage stability evaluation using modal analysis," *IEEE Transactions on Power Systems*, vol. 7, no. 4, pp. 1529-1542, Jul. 1992.

[30] M. Oluic, B. Berggren, F. M. Echavarren *et al*., "On the nature of voltage impasse regions in power system dynamics studies," *IEEE Transactions on Power Systems*, vol. 33, no. 3, pp. 2660-2670, May 2018.

[31] L. S. Neves and L. F. Costa Alberto, "On the computation of the locally closest bifurcation point considering loading uncertainties and reactive power limits," *IEEE Transactions on Power Systems*, vol. 35, no. 4, pp. 3885-3894, Sept. 2020.

Xiaoyu Peng received the B.Sc. degree in electrical engineering from Tsinghua University, Beijing, China, in 2023, where he is currently pursuing the Ph.D. degree. His research interests include stability analysis of phase-angle and voltage dynamics in inverter-dominant power systems.

Feng Liu received the B. Sc. and Ph. D. degrees in electrical engineering from Tsinghua University, Beijing, China, in 1999 and 2004, respectively. He is currently an Associate Professor at Tsinghua University. From 2015 to 2016, he was a Visiting Associate at the California Institute of Technology, Pasadena, USA. His research interests include stability analysis, optimal control, robust dispatch, and game theory-based decision-making in energy and power systems.

Peng Yang received the B.Sc. degree in electrical engineering, the B.Sc. degree in applied mathematics, and the Ph.D. degree in electrical engineering from Tsinghua University, Beijing, China, in 2017, 2018, and 2022, respectively. He is currently an Associate Professor with the School of Electronics and Information, Xi'an Polytechnic University, Xi'an, China. His research interests include power system stability analysis and control.

Beisi Tan is a Senior Engineer with the North China Branch, State Grid Corporation of China, Beijing, China. His research interest includes control of power systems with large-scale renewable energy integration.

Pengfei Gao is a Senior Engineer with the North China Branch, State Grid Corporation of China, Beijing, China. His research interest includes control of power systems with large-scale renewable energy integration.

Zhaojian Wang received the B. Sc. degree in electrical engineering from Tianjin University, Tianjin, China, in 2013, and the Ph.D. degree in electrical engineering from Tsinghua University, Beijing, China, in 2018. From 2016 to 2017, he was a Visiting Ph.D. Student with the California Institute of Technology, Pasadena, USA. From 2018 to 2020, he was a Postdoctoral

Scholar with Tsinghua University. He is currently an Associate Professor at Shanghai Jiao Tong University, Shanghai, China. His research interests include stability analysis, optimal control, and vehicle to grid regulation and game theory based decision-making in energy and power systems.